chemosensors

MDPI

Article

Spinel Magnesium Ferrite ($MgFe_2O_4$): A Glycine-Assisted Colloidal Combustion and Its Potentiality in Gas-Sensing Application

Digambar Nadargi [1,*], Ahmad Umar [2,3,*,†], Jyoti Nadargi [4], Jayvant Patil [1], Imtiaz Mulla [5], Sheikh Akbar [3] and Sharad Suryavanshi [1,*]

[1] School of Physical Sciences, Punyashlok Ahilyadevi Holkar Solapur University, Solapur 413255, India
[2] Department of Chemistry, Faculty of Science and Arts and Promising Centre for Sensors and Electronic Devices (PCSED), Najran University, Najran 11001, Saudi Arabia
[3] Department of Materials Science and Engineering, The Ohio State University, Columbus, OH 43210, USA
[4] Department of Physics, Santosh Bhimrao Patil College, Mandrup, Solapur 413221, India
[5] Former Emeritus Scientist (CSIR), NCL, Pune 411008, India
* Correspondence: nadargidigambar@gmail.com (D.N.); ahmadumar786@gmail.com (A.U.); sssuryavanshi@rediffmail.com (S.S.)
† Visiting Professor at the Ohio State University, Columbus, OH 43210, USA.

Abstract: Herein, we describe the facile synthesis of spinel $MgFe_2O_4$ ferrite and its potential use as a gas sensor using a straightforward and reliable sol–gel approach, i.e., the glycine-assisted auto-combustion route. The novelty in obtaining the sensing material via the auto-combustion route is its inherent simplicity and capability to produce the material at an industry scale. The said cost-effective process makes use of simple metal salts (Mg and Fe-nitrates) and glycine in an aqueous solution, which leads to the formation of spinel $MgFe_2O_4$ ferrite. A single-phase crystallinity with crystallite sizes ranging between 36 and 41 nm was observed for the synthesized materials using the X-ray diffraction (XRD) technique. The porous morphologies of the synthesized materials caused by auto-ignition during the combustion process were validated by the microscopic investigations. The EDS analysis confirmed the constituted elements such as Mg, Fe, and O, without any impurity peaks. The gas-sensing ability of the synthesized ferrites was examined to detect various reducing gases such as LPG, ethanol, acetone, and ammonia. The ferrite showed the highest response (>80%) toward LPG with the response and recovery times of 15 s and 23 s, respectively. Though the sensor responded low toward ammonia (~30%), its response and recovery times were very quick, i.e., 7 s and 9 s, respectively. The present investigation revealed that the synthesized ferrite materials are good candidates for fabricating high-performance sensors for reducing gases in real-world applications.

Keywords: $MgFe_2O_4$; glycine combustion; gas sensors; reducing gases

check for updates

Citation: Nadargi, D.; Umar, A.; Nadargi, J.; Patil, J.; Mulla, I.; Akbar, S.; Suryavanshi, S. Spinel Magnesium Ferrite ($MgFe_2O_4$): A Glycine-Assisted Colloidal Combustion and Its Potentiality in Gas-Sensing Application. *Chemosensors* **2022**, *10*, 361. https://doi.org/10.3390/chemosensors10090361

Academic Editor: Marco Frasconi

Received: 2 August 2022
Accepted: 5 September 2022
Published: 9 September 2022

1. Introduction

In a globalized automated life style, sensors play a key role in the comfort-with-safety segment of human life. In the IoT (Internet of Things) development and extensive use in smart home and smart city programs, sensors are directing other technologies to improve the quality of life of individuals across the globe. Traditionally, gas sensors were restricted to the detection of accidental discharge of gases in the industry sector and leak detection in households. A growing challenge of environmental sustainability due to pollution and increased greenhouse gas emissions led to the development of gas sensor research and development. However, a new ecosystem for environmental monitoring is being made possible by a fresh wave of miniaturization and cost reduction in the gas sensor industry. The value of this asset, according to analysts at ID-Tech Ex, is expected to be USD 361 million in 2017, USD 2.4 billion in 2022, and more than USD 3 billion in 2027 [1]. In view of this, amongst the various gas sensors such as electrochemical sensors, metal oxide

sensors, and optical particle monitoring, metal oxide sensors possess many advantages such as easy production, low cost, and compact size.

In the state of the art, metal oxides such as SnO_2, ZnO, WO_3, CuO, and In_2O_3 are potential gas-sensing materials. There is an unprecedented volume of work being conducted using nano-heterostructured oxides for gas sensing. For example, Wang et al. reported a highly sensitive acetone gas sensor based on PtCu-modified WO_3. The obtained hollow spheres with 0.02% PtCu loading displayed high sensitivity (204.9 tower 50 ppm CH_3COCH_3), good selectivity, and fast response/recovery speeds (3.4 s/7.5 s) at a very low detection limit (0.01 ppm) [2]. In terms of ZnO, recently, Xin-Zhen and his co-workers reported porous Zn_2TiO_4-ZnO microtubes for acetone sensing [3]. The developed microtubes showed excellent acetone-sensing performance with a response of 33.4 for 100 µg/mL acetone, with 6 and 16 sec response and recovery times, respectively. Regarding ferrite-type metal oxides, Zhang et al. reported the development of $CuFe_2O_4$ hollow microspheres for NH_3/TMA sensing at low working temperatures. The response to 10×10^{-6} NH_3 was 4.0 with a rapid response time of 32 sec and a response of 3.95 to TMA [4].

Their detection principle is based on the change in conductivity upon interaction with a chemical species at the sensor surface, which is generally transition metal ferrites (e.g., Mn, Mg, Zn, Ni, Co, and Cd) with an AB_2O_4 formula [5–13]. We quote the term "easy production" as one of its merits, amongst all the adopted synthetic routes, because the glycine combustion process is a highly promising route because of several factors. The factors include the ability to precisely control how the constituent ions are mixed, low combustion heat (3.24 kcal/g), a self-propagating chemical mechanism, and many others. Additionally, glycine functions as a fuel for combustion as well as a component of a complex with metal ions that prevent the formation of selective precipitations [14,15].

Dalt et al. reported the synthesis of nanostructured $MgFe_2O_4$ ferrites using glycine as fuel, and the observed results of the magnetic and structural characterizations reveal that the material was ferromagnetic at room temperature [16]. The nanostructured $MgFe_2O_4$ powder with a varying degree of oxidizers (metal nitrates) was synthesized using a glycine-based solution-combustion route by V. Rajendar et al. [17]. Deraz et al. reported the synthesis of nano-magnetic magnesium ferrite particles using the glycine auto-combustion route, where physicochemical properties of the material were investigated [18]. Little to no work has been conducted on $MgFe_2O_4$ as a gas-sensing material [18,19].

The present study focused on fabricating a compact-size gas sensor based on spinel $MgFe_2O_4$ ferrite material via the glycine combustion process. Moreover, a varying degree of oxidizer (Fe-nitrate) with respect to oxygen ($MgFe_{2-x}O_{4-\delta}$, x = 0, 0.05, and 0.1) was investigated against the gas response competence at different operating temperatures ranging from 475 to 725 K. Furthermore, the ferrite preparation strategy was described in relation to the structural and morphological research.

2. Experimental Details

2.1. Materials Used

To synthesize the ferrite materials, glycine ($C_2H_5NO_2$), magnesium ($Mg(NO_3)_2$ $6H_2O$), and ferric nitrate ($Fe(NO_3)_3$ $9H_2O$) were employed as procured without any further processing. All chemicals were of reagent grade and procured from S.D. fine chemicals.

2.2. Synthesis Protocol

In a typical synthesis process, the necessary amount of glycine was added after the stoichiometric amount of nitrate salts (3:5 moles, based on the total oxidizing and reducing valence of the oxidizer and reductant) which had been dissolved in double-distilled water. The reaction mixture was stirred well to produce a homogenous solution, and then the obtained solution was heat treated roughly to 425 K. The viscosity of the solution gradually rose while staying within the bounds of the natural law (Figure 1a). However, once the percolation threshold was crossed, the viscosity increased, and the solution entered the jelly phase (no-liquid state). The resulting gel underwent additional heat treatment at a

slightly higher temperature (450–475 K). This induced the frothing of the gel, with the evaporation of water molecules from the gel body. The gel began draining into a rapid flameless auto-combustion reaction with the evolution of significant amounts of gaseous products not long after the water molecules had completely evaporated. The process started from the hottest zones of the reaction mixture, ending in voluminous $MgFe_2O_4$ xerogel powder. The raw powder was then calcined in air for 2 h at 775 K to remove any remaining unreacted salt species and their byproducts (if any), yielding the pure compound.

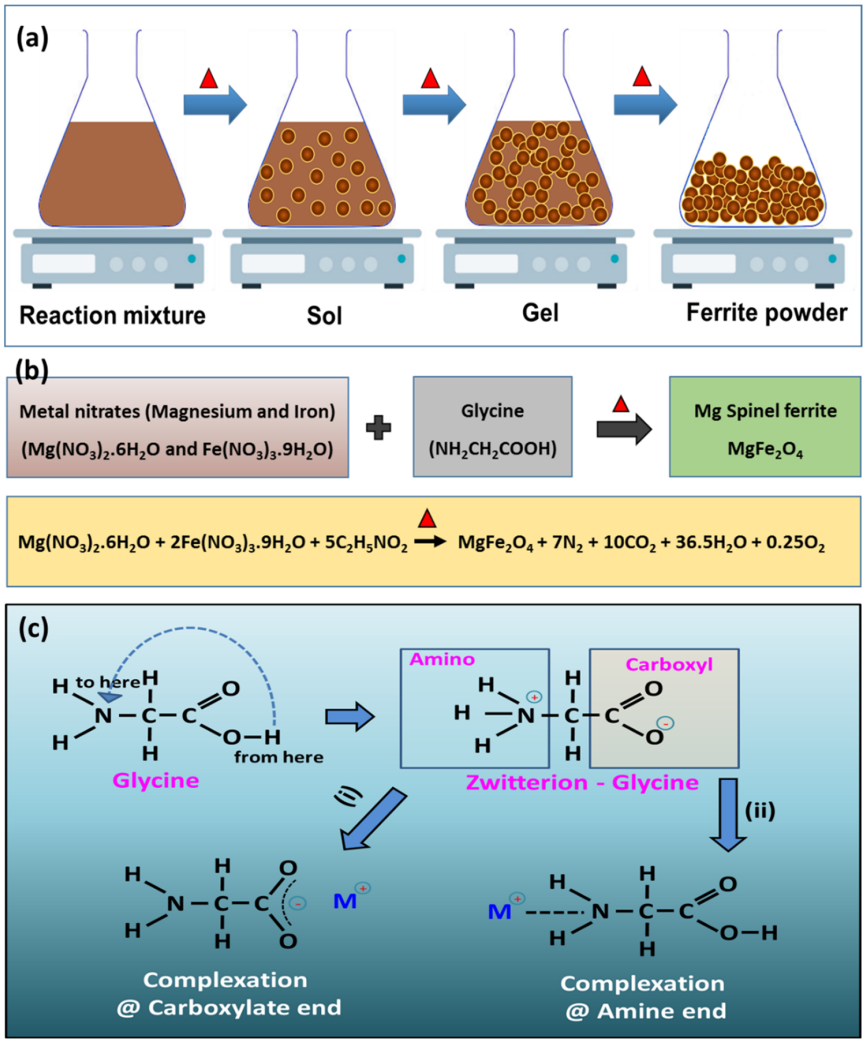

Figure 1. Schematic illustration of (**a**) preparation of ferrite powder, (**b**) reaction mechanism of $MgFe_2O_4$, and (**c**) zwitterion characteristics of glycine, respectively.

2.3. Characterization Techniques

To identify the crystal structure of $MgFe_2O_4$ powder, XRD (Bruker D2 with CuKα-1 radiations of wavelength 1.5406 Å) was utilized. The morphological and elemental distribution analysis of the developed ferrites were studied by FESEM with EDAX (HITACHI SU5000). The gas-sensing analysis of the ferrites is described in the following sub-section.

2.4. Sensor Design and Measurement

Due to the compact size of the sensor, the as-synthesized ferrite materials were deposited on the electrode surface using a screen-printing technique as thick films. For this, a temporary binder (ethyl cellulose and butyl carbotyl acetate) was used to prepare the thixotropic paste of calcined $MgFe_2O_4$ powder. The thick films were then heat treated at 973 K for 2 h.

The resistance of the thick films in air and with test gas was determined as a function of time at various operating temperatures and test gas concentrations. The formula used to determine the gas response was as follows:

$$S\ (\%) = \frac{R_a - R_g}{R_a} \times 100 \quad (1)$$

where R_a and R_g, respectively, represent the sensor's resistance in the absence of test gas and the presence of air. Through the repeatability and reproducibility of the studies, the performance of the fabricated sensors was validated.

3. Results and Discussion

The formation of ferrite with magnesium from their respective metal salts is highlighted in Figure 1b. Here, glycine acts as a gelation agent as well as fuel, through a redox reaction. The initial reactions produce metal hydroxides, which then go through polycondensation to produce polymeric or cluster-like polyoxometallates. These clusters undergo structural and temporal evolution, resulting in a colloidal gel of iron–magnesium metal oxide nanoparticles [20].

Regarding the role of glycine, it has zwitterion (meaning "dual" in German) characteristics. Two distinct end groups, namely carboxylic (–COOH) and amino ($–NH_2$), can be used to create complexes [21–23]. It forms a complex with the relevant metal ions by functioning as a bidentate ligand (a ligand having two teeth or atoms that coordinate straight to the central metal atom). Moreover, it increases the solubility of metal ions, hence preventing selective precipitation. Figure 1c illustrates the aforementioned feature of glycine in generating a stable metal complex.

3.1. Crystallographic Properties of the Prepared Ferrite Materials

By using grazing incidence X-ray diffraction, the crystal structure of annealed $MgFe_{2-x}O_{4-\delta}$ (x = 0, 0.05, and 0.1) films was confirmed (Figure 2). The ferrite films had the very same Bragg reflection characteristics that are indicative of the spinel $MgFe_2O_4$ structure. The relative strengths of the various reflections resulting from various crystal plane reflections correspond to (2 2 0), (3 1 1), (4 0 0), (422), (5 1 1), and (4 4 0), clearly confirming the formation of single-phase spinel-type $MgFe_2O_{4-\delta}$. The values of the d-spacing and average lattice parameters match those in the JCPDS files for $MgFe_2O_4$ (No. 73-1720). Table 1 shows the average crystallite size and average lattice parameter of stoichiometric and non-stoichiometric ferrite material. Because the ionic radius of Mg^{2+} ions is higher (0.64 Å) than that of Fe^{3+} ions (0.72 Å), the linear increase in the lattice constant with the x value indicates the lack of Fe^{3+} ions. The improvement in the average crystallite size is attributed to following Vegard's law [24]. The crystal development was constrained by the lower phase formation of stoichiometry, which favored its use in gas sensing.

3.2. Surface Morphological Analyses by FE-SEM

Under SEM examinations, the colloidal method of forming a porous network structure was investigated. The FE-SEM micrographs of stoichiometric and non-stoichiometric ferrite material are shown in Figure 3. All the samples displayed a porous network structure with discrete morphology, except for stoichiometric composition where organized connectivity of the grains was observed (Figure 3a). As the stoichiometry of the ferrite was disturbed, the network structure collapsed and led to the loss of grain connectivity (Figure 3b,c). This agglomeration seems to increase with successive non-stoichiometry [25]. Though the observed morphology puts restrictions on defining the shape and size of the grains, the average grain size was observed to be less than 0.1 µm, indicating the nanocrystalline material.

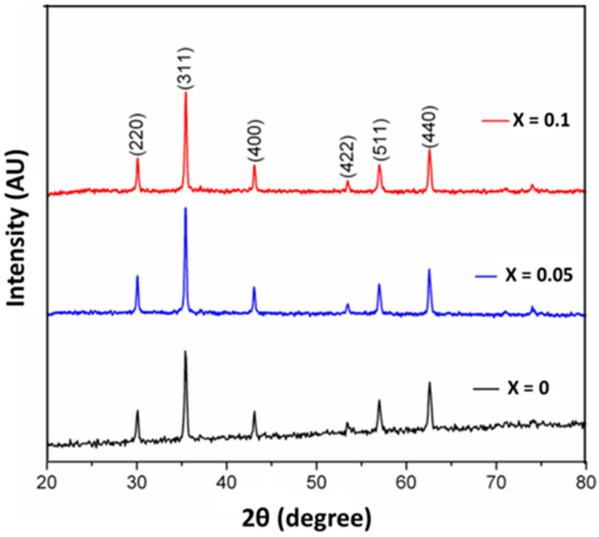

Figure 2. The XRD pattern of heat-treated $MgFe_{2-x}O_{4-\delta}$ (x = 0, 0.05, and 0.1) materials.

Table 1. The crystallite size and lattice parameter of $MgFe_{2-x}O_{4-\delta}$ (x = 0, 0.05, and 0.1) materials.

Sample ID	Crystallite Size (nm)		Lattice Parameter of Heat-Treated Sample "a"
	As-Prepared	Heat-Treated	
$MgFe_2O_4$	30	36	8.36
$MgFe_{1.95}O_{4-\delta}$	34	41	8.38
$MgFe_{1.9}O_{4-\delta}$	35	40	8.39

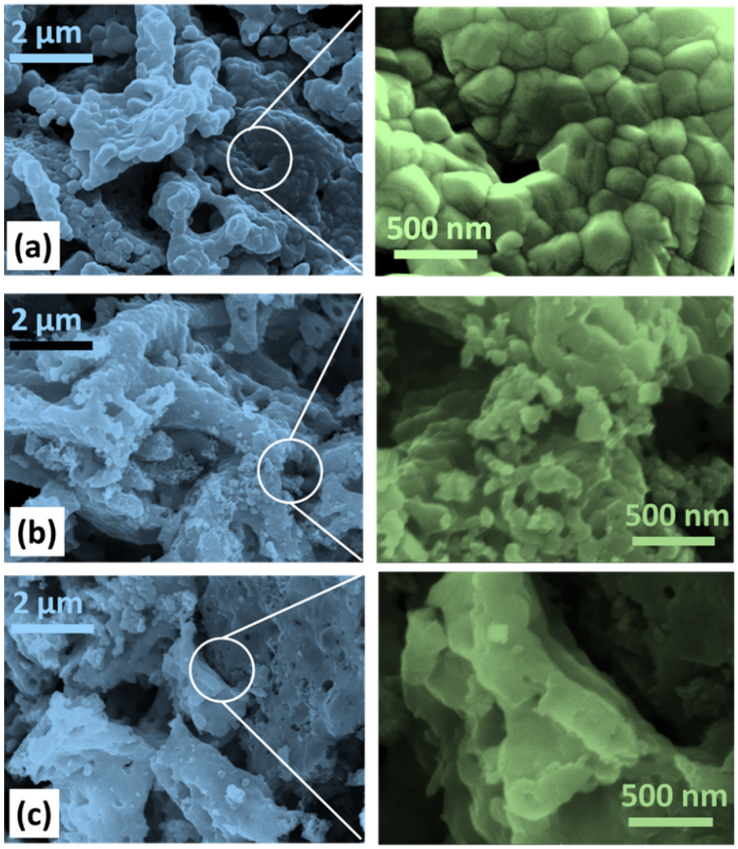

Figure 3. SEM images of $MgFe_{2-x}O_{4-\delta}$ (x = 0 (**a**), 0.05 (**b**), and 0.1 (**c**)) ferrite, respectively.

3.3. Elemental Analyses by EDS

Following morphological investigations, elemental analysis/chemical characterization of as-developed material was carried out using EDS analysis, and the results are shown in Figure 4a–c. The observed EDS spectra for the prepared ferrite materials clearly confirmed the presence of various elements, i.e., Mg, Fe, and O. The corresponding EDS data analysis (Table 2) indicates nearly 1:2 atomic ratios of Mg and Fe with a slightly lower oxygen content and is in good accord with the initial precursor concentration. This clearly indicates that the non-stoichiometric compound ($MgFe_{1.95}O_{4-\delta}$) was achieved using the presented simple and facile synthesis process.

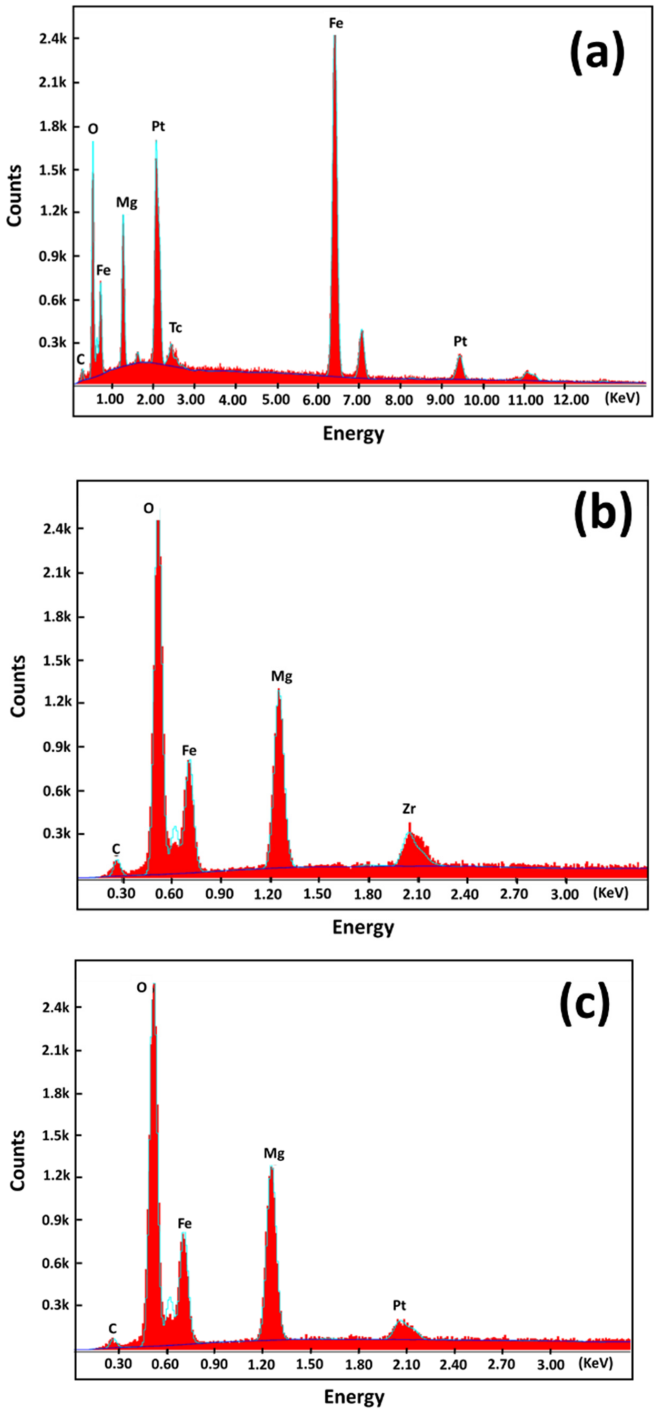

Figure 4. EDS spectra of $MgFe_{2-x}O_{4-\delta}$ (x = 0 (**a**), 0.05 (**b**), and 0.1 (**c**)) ferrite, respectively.

Table 2. EDS quantitative analysis of $MgFe_{2-x}O_{4-\delta}$ (x = 0, 0.05, and 0.1) materials.

Element	$MgFe_{2-x}O_{4-\delta}$ (x = 0)		$MgFe_{2-x}O_{4-\delta}$ (x = 0.05)		$MgFe_{2-x}O_{4-\delta}$ (x = 0.1)	
	Wt%	At%	Wt%	At%	Wt%	At%
O	18.02	39.54	19.43	41.03	53.71	68.09
Mg	10.94	15.80	13.01	18.08	37.08	30.95
Fe	71.03	44.65	67.55	40.88	9.19	0.95

3.4. Gas-Sensing Properties

It is widely known that the capacity of a material to detect gases depends on its porosity, surface microstructure, surface-to-volume ratio, and grain size [26]. As is well known, all these properties are directly linked to the method of preparation of the material. Following one of our objectives, the prepared material using glycine colloidal chemistry was evaluated for its gas-sensing behavior. LPG, acetone, ethanol, and ammonia (the four most prevalent reducing gases encountered in daily life) were all evaluated for this purpose at various operating temperatures and concentrations. The material showed the gas-sensing behavior for all the reducing test gases, which is depicted in Figure 5a.

In general, the highest response to each reducing gas coincided with a particular temperature). According to the response characteristics, the sensor exhibits a strong response to LPG at an operating temperature of 648 K. However, it decreased in the higher temperature region. For acetone and ethanol, a large operating temperature range (550–675 K) with a nearly consistent response was observed. The maximum response for the fabricated sensor to LPG, ethanol, and ammonia was 82, 61, and 35%, respectively, at the operating temperature of 648 K. In addition, the maximum response to acetone was 69% at 673 K. Further, it can be seen that $MgFe_2O_4$ displayed typical n-type semiconducting behavior because the resistance of the sensor decreased after being exposed to the reducing gas.

It is well known that the electrical properties of ferrites are strongly dependent on the stoichiometry of the material [27]. The compounds generally have oxygen vacancies or excess oxygen in their lattice. The electrical properties are influenced by the amount of oxygen, and the oxygen vacancies provide useful surface states for the adsorption of oxygen [28]. As the adsorption of oxygen is one of the main phenomena of the gas-sensing mechanism and it can influence the response of particular material to any reducing gas, the non-stoichiometric ferrites were tested for gas response characteristics. In the nonstoichiometric case $MgFe_{2-x}O_{4-\delta}$ (with x = 0.05, 0.1), as the Fe deficiency in the ferrite increased, the response to all the gases was found to increase with a marginal decrease in the operating temperature. For ferrite $MgFe_{2-x}O_{4-\delta}$ (with x = 0.05), the maximum response of 74% was observed to acetone at an operating temperature of 648 K, whereas it was 75, 68, and 33% for LPG, ethanol, and ammonia at 623, 648, and 623 K, respectively (Figure 5b). The ferrite with x = 0.1 showed the maximum response toward LPG (82% at 623 K) as compared to acetone (81% at 598 K), ethanol (75% at 598 K), and ammonia (31% at 623 K), respectively (Figure 5c). By showing the maximum response to LPG, acetone, and ethanol at different operating temperatures, the sensors showed selective behavior at a particular temperature. Thus, one may use the same sensor to detect several gases by adjusting the working temperature.

Figure 6a–c shows the gas response of the material as a function of test gas concentration at the achieved optimum operating temperature. As observed, all the sensors displayed maximum response toward LPG in contrast to ammonia. As the concentration of LPG was increased from 100 to 500 ppm, the response increased rapidly up to 80% (see inset). Additionally, the sharp rise in response for all gases at the lower concentrations initially can be explained by the transfer of electrons from the conduction band of the grain surface to O_2 according to the following reactions (2) and (3).

$$O_2\ (gas) + e^- \leftrightarrow O_2^-\ (ads) \quad (2)$$

$$O_2^-\ (ads) + 2e^- \leftrightarrow 2O^-\ (ads) \quad (3)$$

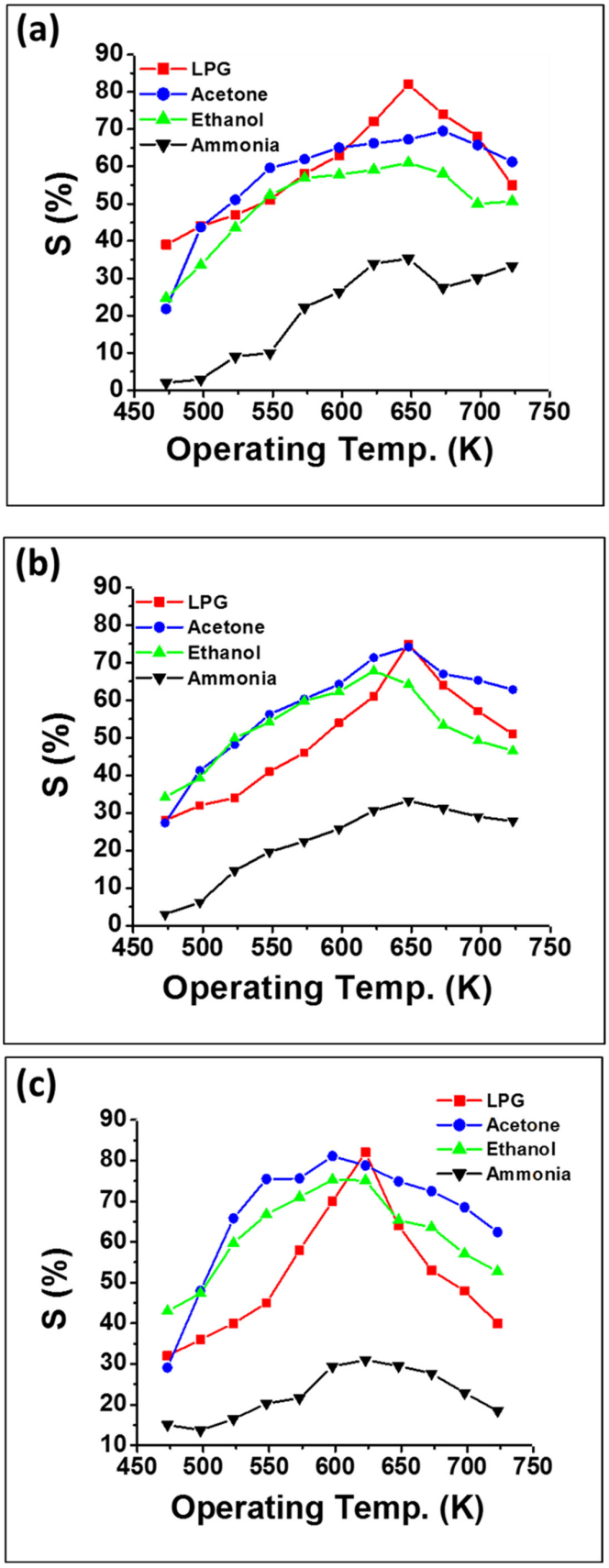

Figure 5. Gas response as a function of operating temperature for $MgFe_{2-x}O_{4-\delta}$ ferrite, (**a**) x = 0, (**b**) x = 0.05, and (**c**) x = 0.1, respectively.

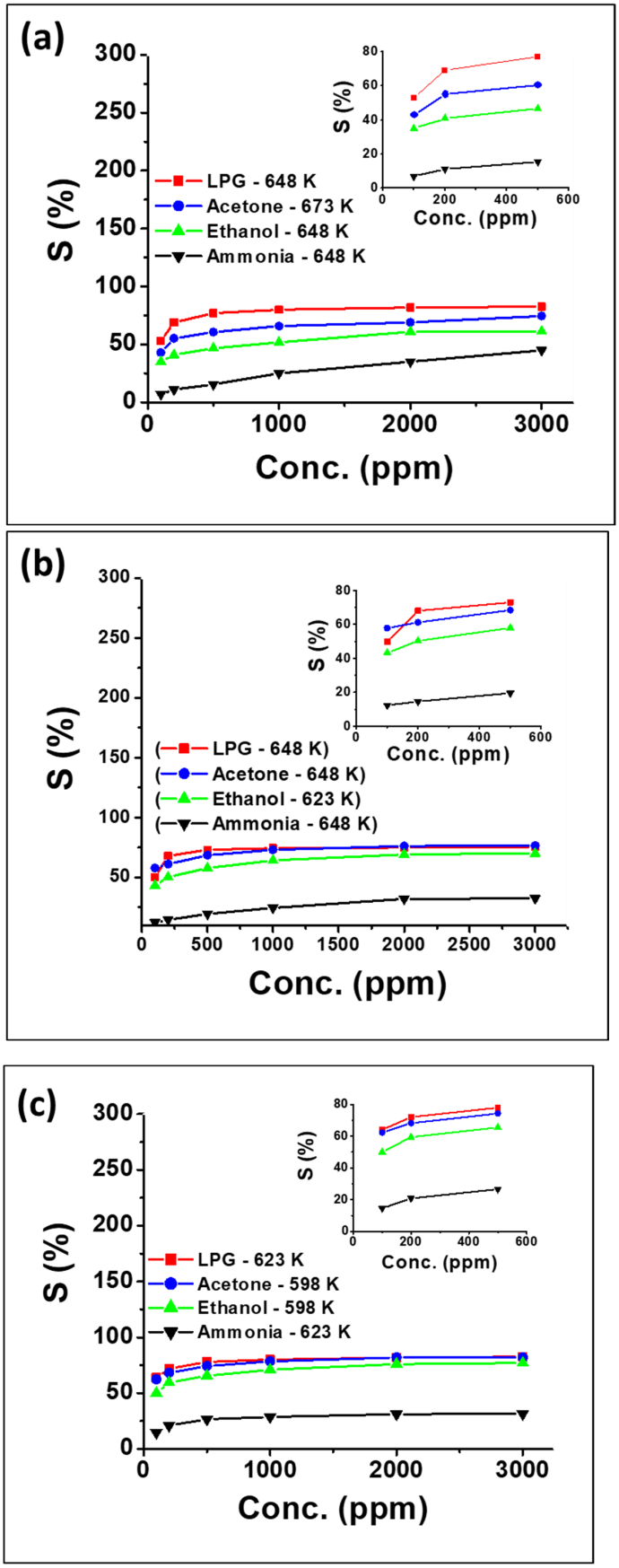

Figure 6. Gas response as a function of concentration of test gases at optimum operating temperature of as-prepared ferrites $MgFe_{2-x}O_{4-\delta}$, (**a**) x = 0, (**b**) x = 0.05, and (**c**) x = 0.1, respectively.

This results in high electrical resistance due to the electron-depleted surface, giving rise to a higher response. Since the depth of the depletion layer depends on the surface coverage of oxygen and the intrinsic electron concentration of the sensor, the depletion layer becomes saturated at larger concentrations [29]. Therefore, as-prepared sensors showed a gradual gas response and attained a steady state, after 500 ppm gas concentrations.

Figure 7 shows the selectivity studies of the developed $MgFe_2O_4$ ferrite. The graph clearly exemplifies the LPG selectivity, along with the potential applicability in acetone, methanol, and ammonia sensing. Its response value (S%) reaches 78% for LPG, 76% for acetone, 60% for ethanol, and 28% for ammonia at a 1000 ppm gas concentration with an operating temperature of 648 K.

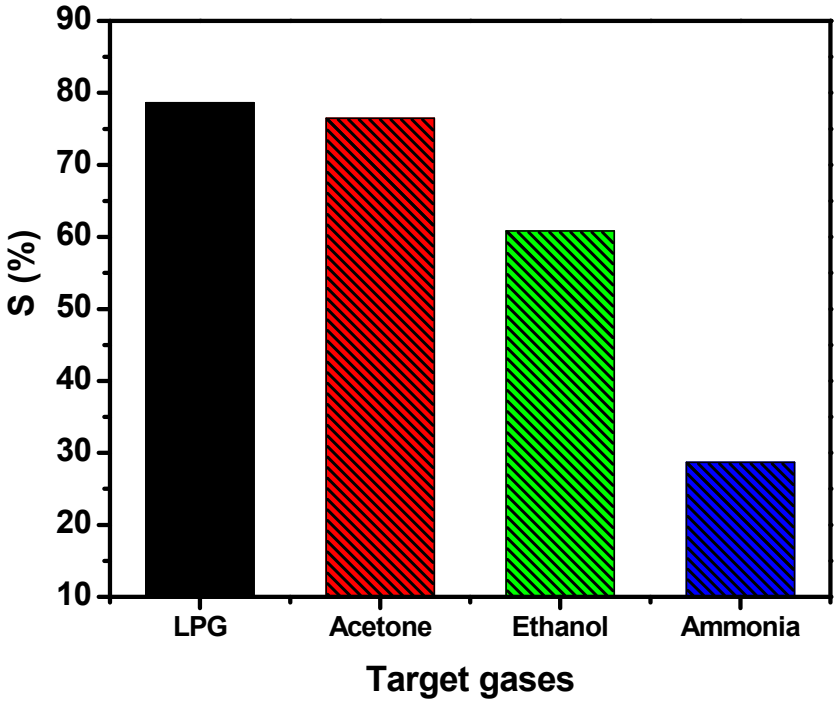

Figure 7. Selectivity test of the developed $MgFe_2O_4$.

In the studies on response and recovery times for test gases, the non-stoichiometric sensor (x = 0.1) showed a short response and recovery times of 9 and 19 s, respectively, for acetone which is noticeably less than the other two compositional sensors. This is attributed to increased operating temperature, which allows for quicker desorption of reaction products and oxygen adsorption, hence decreasing the recovery time for that specific composition. Table 3 lists the response and recovery times for all the fabricated sensors.

Table 3. Response and recovery times of stoichiometric and non-stoichiometric sensor materials toward mentioned reducing gases.

Test Gas	$MgFe_{2-x}O_{4-\delta}$ (x = 0)		$MgFe_{2-x}O_{4-\delta}$ (x = 0.05)		$MgFe_{2-x}O_{4-\delta}$ (x = 0.1)	
	Response Time (s)	Recovery Time (s)	Response Time (s)	Recovery Time (s)	Response Time (s)	Recovery Time (s)
LPG	32	45	15	23	23	41
Acetone	15	33	9	19	15	32
Ethanol	18	30	13	21	18	35
Ammonia	6	14	7	9	8	17

It was discovered that the sensors' stability (shelf life) toward LPG at the conditional parameters was unaffected, displaying 90% of its prior performance even after 60 days. The following Figure 8 displays the stability of the developed $MgFe_2O_4$ over the span of 60 days.

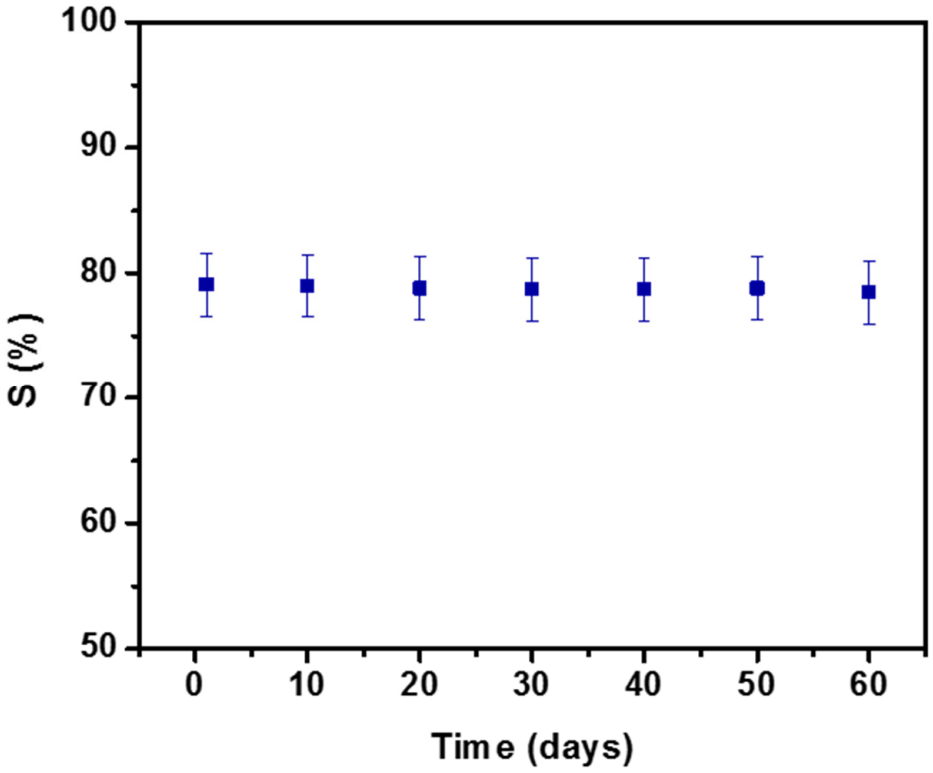

Figure 8. Stability test of the developed $MgFe_2O_4$.

Table 4 provides a performance summary of the fabricated $MgFe_2O_4$ spinel-ferrite-based gas sensor and its comparison with the gas sensors fabricated based on the same $MgFe_2O_4$ spinel ferrite nanomaterials already reported in the literature. Interestingly, the fabricated acetone sensor exhibited better response and recovery times.

Table 4. Comparative chart of gas-sensing performance of developed $MgFe_2O_4$ ferrite with state of art in the same field.

Materials	Test Gas	Sensitivity (%)	Concentration (ppm)	Response Time (s)	Recovery Time (s)	Operating Temp (°C)	Method	Ref.
$MgFe_2O_4$	CO_2	36	5000	120	240	450	Co-precipitation	[12]
$MgCe_xFe_{2-x}O_4$	Acetone	500	100	1.8	249	225	Glyco-thermal technique	[11]
$MgFe_2O_4/BiVO_4$	LPG	58	500	37	42	50	Combustion and hydrothermal methods	[30]
$MgFe_2O_4$	Humidity	10–95% RH	-	18	26	27	Green synthesis	[31]
$MgFe_2O_4/g\text{-}C_3N_4$	Acetone	25	500	49	29	25	Solvothermal method	[32]
$MgFe_2O_4$	Humidity	10–90% RH	-	4	6	25	RF sputtering	[33]
$MgFe_2O_4$	Acetone	80	500	9	19	375	Glycine combustion method	Present work

3.4.1. Gas-Sensing Mechanism in Spinel Ferrites

The well-established semiconductor gas sensor mechanism governs the operation of spinel ferrite gas sensors (Figure 9) [34]. Electrons are trapped when oxygen species chemisorb onto the ferrite particles. This creates a resistance layer on the ferrite particle surface. When chemisorbed oxygen reacts with target gas molecules (for example, acetone), the following reaction occurs when oxygen's electrons are liberated and returned to the ferrite.

$$CH_3COCH_3 + 8O^-_{ads} \rightarrow 3CO_2 + 3H_2O + 8e^- \quad (4)$$

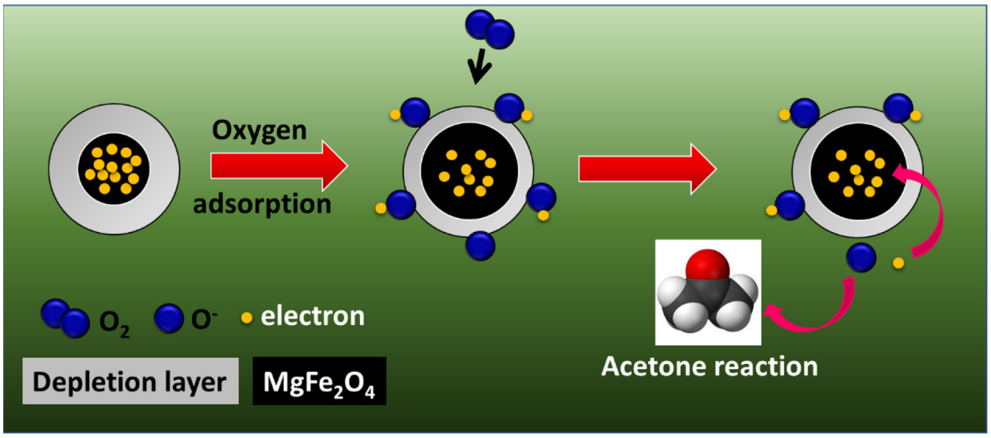

Figure 9. Schematic illustration of acetone gas-sensing mechanism of $MgFe_2O_4$.

The conductivity of the space charge layer is affected by the release of electrons. The conductivity of n-type ferrites increases due to a higher concentration of charge carriers (electrons), but the conductivity of p-type ferrites decreases because electrons recombine with holes. In the following sub-section (Gas-Sensing Mechanism in n-Type Spinel Ferrites, $MgFe_2O_4$), the detailed gas-sensing mechanism in the case of n-type spinel ferrite with an example of $MgFe_2O_4$ is discussed.

Divalent transition metal cations at the octahedral site become oxidized via oxygen chemisorption by spinel ferrites, thus causing a change in the electrical resistance. This is the case for Fe^{2+} in the present ferrite sample, i.e., $MgFe_2O_4$. According to Verwey's theory of charge conduction, transition metal cations from the same element that are positioned in octahedral locations exhibit hopping-type conductivity. The possible hopping is as follows:

$$M^{3+} + e^- \leftrightarrow M^{2+} (\text{for n} - \text{type spinel ferrites}) \quad (5)$$

$$M^{2+} + h^+ \leftrightarrow M^{3+} (\text{for p} - \text{type spinel ferrites}) \quad (6)$$

The cationic conductivity can be increased by increasing the number of M^{2+} and M^{3+} pairs of the same element. Trivalent cations are formed when divalent cations are oxidized during oxygen chemisorption. Depending on the type of cation, test gas lowers trivalent cations back to their divalent form, increasing or decreasing conductivity in spinel ferrites. This variation in the concentration of transition metal cations at octahedral sites affects both the thickness of the space charge layer and the quantity of chemisorbed oxygen. Because M^{2+} is more readily oxidized at the surface as its concentration rises, the space charge layer's thickness is reduced [35].

3.4.2. Gas-Sensing Mechanism in n-Type Spinel Ferrites, $MgFe_2O_4$

The number of Fe^{2+} and Fe^{3+} couples is somewhat smaller than their stoichiometric composition prior to oxygen chemisorption in the octahedral locations of n-type spinel ferrite gas sensors. The conductivity of e^- that hops between iron cations occupying octahedral positions provides charge carrier transfer in n-type spinel ferrites. The electrical conductivity rises as Fe^{2+} concentration increases.

$$Fe^{3+} + e^- \leftrightarrow Fe^{2+} \quad (7)$$

After the chemisorption of oxygen on the n-type spinel ferrite, Fe^{2+} is oxidized to Fe^{3+}. Because of the reduction of Fe^{3+} to Fe^{2+} that occurs when oxygen interacts with the target gas, the material's electrical conductivity and the quantity of Fe^{3+} and Fe^{2+} pairs increase. On the surface of n-type spinel ferrite, these oxidation–reduction reactions are shown to be reversible [36]. $ZnFe_2O_4$, $CdFe_2O_4$, and $MgFe_2O_4$ are the most often used n-type spinel ferrite gas sensors. In the present case of $MgFe_2O_4$ ferrite, in the synthesis or annealing

stages, the Fe^{2+} concentration can be set. The production of iron-excess compounds or annealing in a reducing environment [37] can both preserve ferrous iron. Mg cations are replaced by Fe^{3+}, which moves to tetrahedral positions when iron-excess Mg ferrites are formed.

$$\left(Mg^{2+}_{1-x}\ Fe^{3+}_{x}\right)\left[Fe^{3+}_{2-x}\ Fe^{2+}_{x}\right]\ O_4$$

The quantity of Fe^{2+} can be increased by increasing the iron concentration in a sample [38]. However, if the Fe^{2+} concentration is too high, the Debye length is shortened, and the sensor's responsiveness to gas is reduced [35]. It is possible for oxygen vacancies to form during annealing in a reducing environment; these vacancies are made up by reducing Fe^{3+} to Fe^{2+}.

4. Conclusions

In conclusion, a facile synthesis route of fabricating spinel-type nanocrystalline $MgFe_2O_4$ ferrite was developed using a single-step auto-combusted sol–gel process. The process utilizes metal salts (precursor) and glycine as fuel. For compacting the size of the sensor, the ferrite films are developed using the screen printing technique, and their gas-sensing characteristic is readily controlled by the stoichiometry of the compound. The sensors with non-stoichiometric composition (x = 0.05, and 0.1) display excellent gas-sensing properties toward reduced gases, in comparison with x = 0. The gas response depends on the porosity, stoichiometry, gas type, and operating temperature of the prepared ferrite materials. With regard to ammonia, the sensor with x = 0.05 displayed a quick response (7 s) and a strong recovery (9 s). On the structural, morphological, and gas-sensing properties, the impact of stoichiometry was examined. The larger ionic radius of Mg^{2+} ions was observed to cause an increase in the average crystallite size with non-stoichiometry. From SEM examination, it was obvious that a significant difference in grain formation was seen. The as-developed ferrite showed good response (6–32 s) and recovery times (8–45 s) toward various test gases at diverse temperatures. Thus, it can be used to detect various reduced gases. Last but not least, the method for making gas sensors described here is simple to duplicate and relatively inexpensive, which holds great potential for future industrial applications in gas-sensing technology.

Author Contributions: Writing—original draft preparation: D.N.; writing—review and editing: A.U.; Conceptualization: S.S.; Methodology, validation: J.N.; formal analysis, investigation: J.P.; supervision: I.M.; supervision, resources, visualization: S.A. All authors have read and agreed to the published version of the manuscript.

Funding: This research received no external funding.

Informed Consent Statement: Not applicable.

Acknowledgments: Digambar Nadargi acknowledges UGC D. S. Kothari Postdoctoral Fellowship Scheme, India, for awarding Post-Doctoral Fellowship (No. F.42/2006(BSR)/PH/19–20/0013).

Conflicts of Interest: The authors declare no conflict of interest.

References

1. Chansin, G.; Pugh, D. Environmental Gas Sensors 2017–2027: Technologies, Manufacturers, Forecasts. Scientific Report. 2017. Available online: www.idtechex.com/research/reports/environmental-gas-sensors-2017-2027-000500.asp (accessed on 1 August 2022).
2. Deng, L.; Bao, L.; Xu, J.; Wang, D.; Wang, X. Highly sensitive acetone gas sensor based on ultra-low content bimetallic PtCu modified WO_3_H_2O hollow sphere. *Chin. Chem. Lett.* **2020**, *31*, 2041–2044. [CrossRef]
3. Chen, X.; Wang, X.; Liu, F.; Zhang, G.; Song, X.; Tian, J.; Cui, H. Fabrication of porous Zn_2TiO_4–ZnO microtubes and analysis of their acetone gas sensing properties. *Rare Met.* **2021**, *40*, 1528–1535. [CrossRef]
4. Wu, K.; Xu, J.; Debliquy, M.; Zhang, C. Synthesis and NH_3/TMA sensing properties of $CuFe_2O_4$ hollow microspheres at low working temperature. *Rare Met.* **2021**, *40*, 1768–1777. [CrossRef]
5. Nagarajan, V.; Thayumanavan, A. $CdFe_2O_4$ films for electroresistive detection of ethanol and formaldehyde vapors. *Microchim. Acta* **2018**, *185*, 319–328. [CrossRef]

6. Alharthy, R.D.; Saleh, A. A Novel trace-level ammonia gas sensing based on flexible pani-$CoFe_2O_4$ nanocomposite film at room temperature. *J. Polym. Sci.* **2021**, *13*, 3077–3097. [CrossRef]
7. Zhang, Y.; Jia, C.; Wang, Q.; Kong, Q.; Chen, G.; Guan, H.; Dong, C. MOFs-derived porous $NiFe_2O_4$ nano-octahedrons with hollow interiors for an excellent toluene gas sensor. *J. Nanomater.* **2019**, *9*, 1059–1073. [CrossRef]
8. Zhang, H.; Hu, J.; Li, M.; Li, Z.; Yuan, Y.; Yang, X.; Guo, L. Highly efficient toluene gas sensor based on spinel structured hollow urchin-like core-shell $ZnFe_2O_4$ spheres. *Sens. Actuators B* **2021**, *349*, 130734. [CrossRef]
9. Deivatamil, D.; Mark, J.A.M.; Raghavan, T.; Jesuraj, J.P. Fabrication of $MnFe_2O_4$ and Ni: $MnFe_2O_4$ nanoparticles for ammonia gas sensor application. *Inorg. Chem. Commun.* **2021**, *123*, 108355–108362.
10. Patil, J.Y.; Nadargi, D.Y.; Mulla, I.S.; Suryavanshi, S.S. Cerium doped $MgFe_2O_4$ nanocomposites: Highly sensitive and fast response-recoverable acetone gas sensor. *Heliyon* **2019**, *5*, e01489. [CrossRef]
11. Mkwae, P.; Kortidis, I.; Kroon, R.E.; Leshabane, N.; Jozela, M.; Swart, H.C.; Nkosi, S.S. Insightful acetone gas sensing behaviour of Ce substituted $MgFe_2O_4$ spinel nano-ferrites. *J. Mater. Res. Technol.* **2020**, *9*, 16252–16269. [CrossRef]
12. Sumangala, T.P.; Pasquet, I.; Presmanes, L.; Thimont, Y.; Bonningue, C.; Venkataramani, N.; Prasad, S.; Baco-Carles, V.; Tailhades, P.; Barnabé, A. Effect of synthesis method and morphology on the enhanced CO_2 sensing properties of magnesium ferrite $MgFe_2O_4$. *Ceram. Int.* **2018**, *44*, 18578–18584.
13. Karuppasamy, K.; Sharma, B.; Vikraman, D.; Jo, E.B.; Sivakumar, P.; Kim, H.S. Switchable p-n gas response for 3D-hierarchical $NiFe_2O_4$ porous microspheres for highly selective and sensitive toluene gas sensors. *J. Alloys Compd.* **2021**, *886*, 161281–161290. [CrossRef]
14. Godbole, R.V.; Rao, P.; Alegaonkar, P.S.; Bhagwat, S. Influence of fuel to oxidizer ratio on LPG sensing performance of $MgFe_2O_4$ nanoparticles. *Mat. Chem. Phy.* **2015**, *161*, 135–141. [CrossRef]
15. Patil, J.Y.; Nadargi, D.Y.; Gurav, J.L.; Mulla, I.S.; Suryavanshi, S.S. Synthesis of glycine combusted $NiFe_2O_4$ spinel ferrite: A highly versatile gas sensor. *Mat. Lett.* **2014**, *214*, 144–147. [CrossRef]
16. Dalt, S.D.; Takimi, A.S.; Sousa, V.C.; Bergmann, C.P. Magnetic and structural characterization of nanostructured $MgFe_2O_4$ synthesized by combustion reaction. *Part. Sci. Technol.* **2009**, *27*, 519–527. [CrossRef]
17. Ahmadipour, M.; Rao, K.V.; Rajendar, V. Formation of nanoscale $Mg_{(x)}Fe_{(1-x)}O_4$ (x = 0.1, 0.2, 0.4) structure by solution combustion: Effect of fuel to oxidizer ratio. *J. Nanomat.* **2012**, *2012*, 163909. [CrossRef]
18. Deraz, N.M.; Alarifi, A. Novel preparation and properties of magnesioferrite nanoparticles. *J. Anal. Appl. Pyrolysis* **2012**, *97*, 55–61. [CrossRef]
19. Bangale, S.V.; Bamane, S.R. Nanostructured $MgFe_2O_4$ thick film resistors as ethanol gas sensors operable at room temperature. *Sens. Transd. J.* **2012**, *137*, 176–188.
20. Patil, J.Y.; Khandekar, M.S.; Mulla, I.S.; Suryavanshi, S.S. Combustion synthesis of magnesium ferrite as liquid petroleum gas (LPG) sensor: Effect of sintering temperature. *Curr. Appl. Phys.* **2012**, *12*, 319–324. [CrossRef]
21. Lin, S.; Guo, Y.; Li, X.; Liu, Y. Glycine acid-assisted green hydrothermal synthesis and controlled growth of WO_3 nanowires. *Mater. Lett.* **2015**, *152*, 102–104. [CrossRef]
22. Yin, M.; Yu, L.; Liu, S. Synthesis of thickness-controlled cuboid WO_3 nanosheets and their exposed facets-dependent acetone sensing properties. *J. Alloys Compd.* **2017**, *696*, 490–497. [CrossRef]
23. Mehta, S.; Nadargi, D.; Tamboli, M.; Patil, V.; Mulla, I.; Suryavanshi, S. Macroporous WO_3: Tunable morphology as a function of glycine concentration and its excellent acetone sensing performance. *Ceram. Int.* **2019**, *45*, 409–414. [CrossRef]
24. Bamzai, K.K.; Kour, G.; Kaur, B.; Kulkarni, D. Preparation and structural and magnetic properties of Ca substituted magnesium ferrite with composition $MgCa_xFe_{2-x}O_4$ (x = 0.00, 0.01, 0.03, 0.05, 0.07). *J. Mat.* **2014**, *2014*, 184340. [CrossRef]
25. Eltabey, M.M.; Massoud, A.M.; Radu, C. microstructure and superparamagnetic properties of Mg-Ni-Cd ferrites nanoparticles. *J. Nanomat.* **2014**, *2014*, 492832. [CrossRef]
26. Sun, Y.F.; Liu, S.B.; Meng, F.L.; Liu, J.Y.; Jin, Z.; Kong, L.T.; Liu, J.H. Metal oxide nanostructures and their gas sensing properties: A review. *Sensors* **2012**, *12*, 2610–2631. [CrossRef] [PubMed]
27. Koops, C.G. On the dispersion of resistivity and dielectric constant of some semiconductors at audiofrequencies. *Phys. Rev.* **1951**, *83*, 121–124. [CrossRef]
28. Al-Hashem, M.; Sheikh, A.; Morris, P. Role of Oxygen Vacancies in Nanostructured Metal-Oxide Gas Sensors: A Review. *Sens. Actuators B Chem.* **2019**, *301*, 126845–126855. [CrossRef]
29. Wu, J.; Gao, D.; Sun, T.; Bi, J.; Zhao, Y.; Ning, Z.; Fan, G.; Xie, Z. Highly selective gas sensing properties of partially inversed spinel zinc ferrite towards H2S. *Sens. Actuators B Chem.* **2016**, *235*, 258–262. [CrossRef]
30. Yamazoe, N. New approaches for improving semiconductor gas sensors. *Sens. Actuators B Chem.* **1991**, *5*, 7–19. [CrossRef]
31. Sutka, A.; Mezinskis, G.; Lusis, A.; Jakovlevs, D. Influence of iron non-stoichiometry on spinel zinc ferrite gas sensing properties. *Sens. Actuators B Chem.* **2012**, *172*, 204–209. [CrossRef]
32. Sutka, A.; Mezinskis, G.; Zamovskis, M.; Jakovlevs, D.; Pavlovska, I. Monophasic $ZnFe_2O_4$ synthesis from a xerogel layer by auto combustion. *Ceram. Int.* **2013**, *39*, 8499–8502. [CrossRef]
33. Ayyappan, S.; Raja, S.P.; Venkateswaran, C.; Philip, J.; Raj, B. Room temperature ferromagnetism in vacuum annealed $ZnFe_2O_4$ nanoparticles. *Appl. Phys. Lett.* **2010**, *96*, 143106–143110. [CrossRef]
34. Sutka, A.; Parna, R.; Kleperis, J.; Kambre, T.; Pavlovska, I.; Korsaks, V.; Malnieks, K.; Grinberga, L.; Kisand, V. Photocatalytic activity of non-stoichiometric $ZnFe_2O_4$ under visible light irradiation. *Phys. Scr.* **2014**, *89*, 044011–044020. [CrossRef]

35. Munindra, P.; Reddy, M.B.; Rani, B.G.; Jayarambabu, N.; Kailasa, S.; Rao, P.S.; Rao, K.V. A high-performance low-temperature LPG detection by MgFe2O4/BiVO4 chemiresistive sensor. *J. Mater. Sci. Mater. Electron.* **2020**, *31*, 2370–2377. [CrossRef]
36. Priya, R.S.; Chaudhary, P.; Kumar, E.R.; Balamurugan, A.; Srinivas, C.; Prasad, G.; Yadav, B.C.; Sastry, D.L. Evaluation of structural, dielectric and electrical humidity sensor behaviour of $MgFe_2O_4$ ferrite nanoparticles. *Ceram. Int.* **2021**, *47*, 15995–16008. [CrossRef]
37. Zhang, R.; Wang, Y.; Zhang, Z.; Cao, J. Highly sensitive acetone gas sensor based on g-C3N4 decorated $MgFe_2O_4$ porous microspheres composites. *J. Sens.* **2018**, *18*, 2211–2223. [CrossRef] [PubMed]
38. Kotnala, R.K.; Shah, J.; Mathpal, M.C.; Verma, K.C.; Singh, S.; Lovkush. Influence of annealing on humidity response of RF sputtered nanocrystalline $MgFe_2O_4$. *Thin Solid Films* **2011**, *519*, 6135–6139. [CrossRef]